Cement and Concrete Research 41 (2011) 169–175

Contents lists available at ScienceDirect

Cement and Concrete Research

journal homepage: http://ees.elsevier.com/CEMCON/default.asp

Nanoscale characterization of engineered cementitious composites (ECC)

Aaron Richard Sakulich *, Victor C. Li

Department of Civil and Environmental Engineering, University of Michigan, Ann Arbor, MI, 48109, United States

ARTICLE INFO

Article history:
Received 17 May 2010
Accepted 1 November 2010

Keywords:
ECC
Microstructure (B)
Interfacial transition zone (B)
SEM (B)
Elastic moduli (C)

ABSTRACT

Engineered cementitious composites (ECC) are ultra-ductile fiber-reinforced cementitious composites. The nanoscale chemical and mechanical properties of three ECC formulae (one standard formula, and two containing nanomaterial additives) were studied using nanoindentation, electron microscopy, and energy dispersive spectroscopy. Nanoindentation results highlight the difference in modulus between bulk matrix (~30 GPa) and matrix/fiber interfacial transition zones as well as between matrix and unreacted fly ash (~20 GPa). The addition of carbon black or carbon nanotubes produced little variation in moduli when compared to standard M45-ECC. The indents were observed by electron microscopy; no trace of the carbon black particles could be found, but nanotubes, including nanotubes bridging cracks, were easily located in ultrafine cracks near PVA fibers. Elemental analysis failed to show a correlation between modulus and chemical composition, implying that factors such as porosity have more of an effect on mechanical properties than elemental composition.

1. Introduction

Engineered cementitious composites (ECC) are ultra-ductile fiber-reinforced ordinary Portland cement (OPC)-based composites. The extreme tensile strain capacity of ECC (>3%) is hundreds of times larger than that of ordinary concrete [1]. This ultra ductility is the product of controlled distributed microcracking under tensile forces caused by a low loading (<2 wt.%) of short polymer fibers. The development of ECC has been aided by micromechanical models that predict the behavior of ECC formulae based on fiber/matrix interactions.

The unique properties of ECC are the result of mechanical properties that have their origin on the nanoscale. The most important of these are the fiber/matrix interface, which dictates the behavior of fibers during loading, and the composition of the calcium silicate hydrates (C–S–H) that make up the main binding phase in OPC, which dictates the initiation and behavior of cracks during loading [1]. C–S–H is not a homogeneous material, and occurs in the form of nanoscale grains mixed with nanoscale porosity [2]. High density 'inner product' C–S–H and low density 'outer product' C–S–H [3–5] exist, and have different mechanical properties. A possible third, ultra-high density phase consisting of C–S–H and portlandite has recently been described [6,7].

In addition to ECC formulae containing large quantities of fly ash [8] or granulated ground blast furnace slag [9] for increased sustainability, several ECC formulae containing nanomaterials have been developed. Carbon buckyballs have been investigated as a replacement for super-plasticizers [10] while carbon black and carbon nanotubes are being investigated as methods of altering electrical properties.

Such nanomaterial additives are becoming more and more commonplace in traditional cements. In addition to carbon black and carbon nanotubes [11,12] being used to alter electrical properties, nanoclays have been used in ordinary cement to tailor porosity [2], and titanium dioxide has been used to tailor photocatalytic properties [13]. Other common admixtures, such as superplasticizers and silica fume, have nanoscale attributes.

This study is meant to address three gaps in the current understanding of the behavior of nanomaterial-modified ECC materials: 1) to obtain a more accurate understanding of the mechanical properties of ECC below the microscale; 2) to observe the influence that two nanomaterials (carbon black and single-wall carbon nanotubes) have on these properties, and 3) to attempt to observe the location and disposition of carbon nanotubes, which could theoretically bridge submicron-sized cracks for which micro- or macrofibers are ineffective. Electron microscopy is used here for elemental analysis and to image indentation sites, carbon nanotubes, and general morphology. Microindentation techniques that once made up the bulk of cement indentation research [14,15] have been passed over in favor of nanoindentation techniques that provide information about the nano-scale mechanical properties of cements [3,16–20]. These nanoindentation experiments provide a detailed description of the variation of moduli across the fiber/matrix interface.

2. Materials and methods

2.1. Sample preparation

Three ECC formulae were tested. The first, a basic M45 formula without additives, provided baseline data on the mechanical properties of the various phases in ECC as well as the level of

* Corresponding author. 2350 Hayward St., G.G.Brown Building, Room 1022, Ann Arbor, MI, 48109, United States. Tel.: +1 267 752 8119; fax: +1 734 764 4292.
E-mail address: asakulic@umich.edu (A.R. Sakulich).

0008-8846/$ – see front matter © 2010 Elsevier Ltd. All rights reserved.
doi:10.1016/j.cemconres.2010.11.001

Table 1
Compositions of the three formulae used in this study.

Sample	Cement	Sand	Fly ash	HRWR[a]	Water[b]	Fiber	CB	CNT
M45-ECC	27	22	33	0.4	16	1.3	–	–
CB-ECC	26	22	33	0.4	16	1.3	1	–
CNT-ECC	26.997	22	33	0.4	16	1.3	–	0.003

[a] High range water reducer.
[b] Water to binder ratio of all formulae was 0.267.

variability. Some components of ECC with well known chemical and mechanical properties (quartz, unreacted fly ash, and fibers) were used as standards for nanoindentation and energy dispersive spectroscopy (EDS).

The second formula, CB-ECC, contained 1 wt.% carbon black. The carbon black was added as part of an ongoing research effort to increase the conductivity of ECC, the results of which are to be published elsewhere. To the eye, the carbon black seems well dispersed, as the sample is a uniform dark gray in color. The third formula, CNT-ECC, contained 0.3 wt.% single-walled carbon nanotubes and was also originally produced as part of the above-mentioned study.

The composition of the three formulae used in this study can be found in Table 1. Reactants used include: Type I Portland cement (Holcim Co.) fine silica sand (US Silica) with an average grain size of 110 μm, class F fly ash (Boral Co.) conforming to ASTM C618, high range water reducing admixture (W.R. Grace & Co.), carbon black (Cabot Corp.), single-walled nanotubes (8–15 nm diameter, 500–2000 nm length, Cheaptubes Inc.), and polyvinyl alcohol (PVA) fibers (Kuraray Co.). Due to the strongly hydrophilic nature of PVA, the fiber surfaces were coated with a proprietary oiling agent (1.2% by weight of fiber) by the manufacturer. The chemical compositions of the Portland cement and fly ash used can be found in Table 2.

Batches of ECC were prepared using a Hobart mixer. Specimens were demolded after 24 h, covered with plastic, and cured in the lab at ambient temperature and humidity. All mounting, polishing, and testing occurred after at least 56 days, so as to allow the pozzolanic reaction due to the presence of fly ash to occur.

After curing, samples were cut using a tile saw, mounted in bakelite, and polished using 15, 9, 6, 3, 1, and 0.5 μm diamond solution after grinding with 1200 grit grinding paper (LECO Corp.). Grinding and polishing were performed for 30 s per step (15 N force, 150 rpm complimentary rotation), between which the mounted specimens were rinsed in water and immediately dried. After the final polishing step, the samples were rinsed in ethanol and allowed to dry. The age of the samples (at least 6 months old) and the short period during which they were exposed to water minimized any effect on the level of hydration present in the cement; hydration is relatively 'complete' at such ages and will not be accelerated by brief exposure. After trying a number of different polishing routines, the process described above produced the best results, as determined by electron microscopy (discussed below).

Table 2
Composition of Portland cement and fly ash, as determined by manufacturer and confirmed by EDS.

Composition (wt.%)	Portland cement	Fly ash
CaO	61.8	5.57
SiO_2	19.4	59.5
Al_2O_3	5.3	22.2
Fe_2O_3	2.3	3.9
MgO	0.95	–
SO_3	3.8	0.19
K_2O	1.1	1.11
Na_2O	0.2	2.75
Loss on ignition	2.1	0.21

2.2. Microscopy

Before nanoindentation, optical micrographs were collected (AZ100, Nikon Instruments). These images were used as 'maps' to facilitate choosing indentation locations as well as to identify phases such as fibers, quartz, fly ash, and cementitious matrix. After nanoindentation, these maps were essential to locate indentation sites in the SEM (XL30 FEG SEM, FEI Company). The microscope was fitted with an energy dispersive spectroscopy (EDS) accessory (EDAX Phoenix model, EDAX Inc.). Electron microscopy was performed using low voltages (<5 keV) to reduce beam/sample interaction volume, and at low working distances (between 3 and 5 mm) to improve resolution. Samples were lightly (10 s) sputter coated with a layer of gold to increase conductivity. This layer is unlikely to be thicker than 10 nm, and thus obviates most concerns regarding the distortion of fine details.

2.3. Nanoindentation

Nanoindentation experiments were performed using a device (Nanoindenter II, MTS Nano Instruments, Inc.) fitted with a Berkovitch tip. Tests were carried out in continuous stiffness mode to a predetermined depth (500 nm) with a target drift rate of 0.2 nm/s. An alumina standard was indented during each test to ensure accuracy. Mechanical properties were automatically determined from the unloading segment through methods described by Oliver and Pharr [21]. To account for possible surface roughness, head repositioning was carried out before every indent. Each load/displacement diagram was plotted and inspected for signs of problems due to surface roughness, such as abnormal or discontinuous shapes, etc. Few indents were found that displayed this behavior; those that did were discarded and the data recollected.

3. Results and discussion

3.1. Polishing

The issue of surface roughness is of critical importance to nanoindentation studies. ASTM Standard E2546, developed for indentation testing, states that "the surface finish of the sample will directly affect the test results. The test should be performed on… a suitably prepared surface." [22] Annex E of another standard, ISO 14577, prescribes that the maximum roughness of the sample surface be no more than 1/20th the indentation depth so as to reduce scatter in the results [23]. As the experiments performed here were carried out to a maximum depth of 500 nm, with an estimated final surface roughness of 100 nm, the roughness/depth ratio is 4 times greater than the limit imposed by this standard. This lack of compliance with the limits prescribed in ISO 14557 is a strong factor, combined with cement heterogeneity, in the large standard deviation measured at each point.

The degree to which the ECC can be polished for nanoindentation studies is associated with the microstructure heterogeneity. On the microscale, ECC is composed of several relatively hard phases (quartz, unreacted fly ash, unhydrated cement particles, and mineral impurities) surrounded by a cement matrix. This matrix is extremely heterogeneous on the nanoscale, containing low- and high density C–S–H ('inner product' and 'outer product', respectively), portlandite, ettringite, calcite, mineral impurities, and a variety of pores and voids. Finally, ECC contains a low volume (~2 wt.%) of specially selected, and relatively 'soft,' PVA fibers. It should be noted that the fibers are mechanically anisotropic; the modulus calculated from indents performed perpendicular to the main axis (that is, on a rectangular cross section) is roughly 1/3 that reported by the manufacturer, who tested them along the main axis (~15 GPa vs. 42.8 GPa).

This heterogeneity of the ECC matrix leads to extreme difficulty in polishing. The hardest phases (quartz, fly ash) polish perfectly, to a roughness undetectable by SEM. At low magnification, the many different phases of ECC can be observed by both optical microscopy (Fig. 1a) and SEM (Fig. 1b).

Such difficulties can be overcome with careful polishing. Although exact details of polishing regimens vary from author to author and material to material, the method used here is similar to that used by a number of others for cement [3,4,16,20,24] and for fiber-reinforced composites such as ECC [18,25]. Although an imperfect method, and well outside the limits suggested by ISO 14457, this polishing regime leads to the best surface polish that could be obtained. The inability to obtain an excellent polish is a main factor in the large deviations reported in the indent data.

Surface roughness is beyond the limits of optical microscopy, and when viewed at high magnification in the SEM (Fig. 1c), the roughness is estimated to be on the order of 100 nm, even for the best polishing routine developed. This is relatively high compared to the depth of the nanoindentation experiments (500 nm), however, is still likely to add a certain degree of variability to the results. The results of the nanoindentation experiments performed here, and what they imply about the quality of the sample surfaces polish, is discussed below.

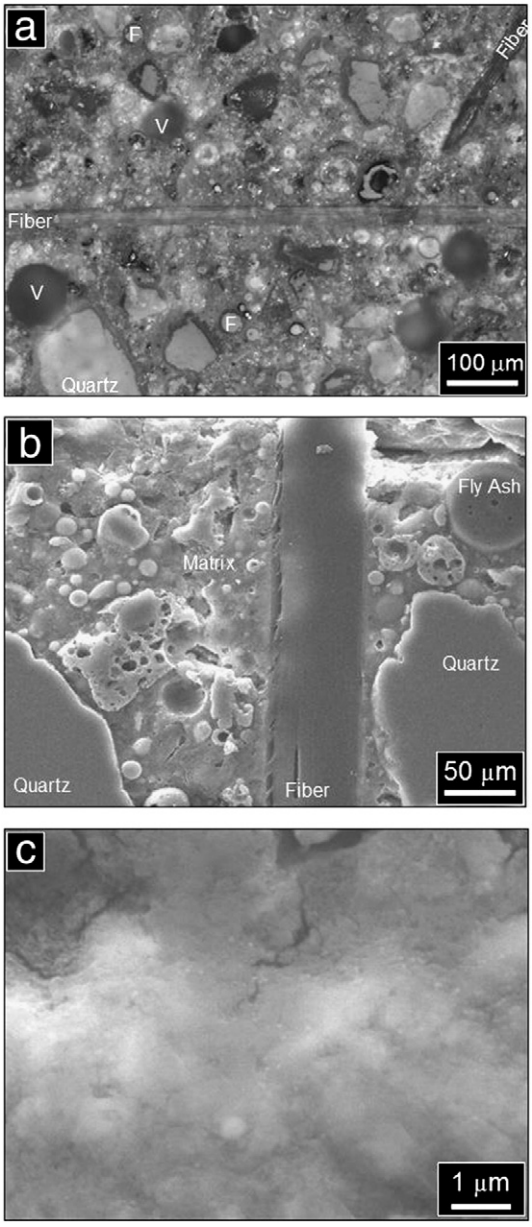

Fig. 1. Polished ECC. a) Optical microscopy, in which fibers, quartz, voids (v), unreacted fly ash (F), and the extremely heterogeneous matrix can be observed. b) Electron microscopy, in which the various microphases can be observed, and roughness of the cement matrix is clearer.

3.2. Nanoindentation

A polished alumina standard, provided by the manufacturer of the indentation apparatus, was indented 10 times to determine the deviation inherent in the machine. The measured modulus (75.7 ± 11.3 GPa) is in good agreement with the actual value (70.4 GPa) but represents a roughly 15% standard deviation.

Nanoindentation data from the literature (Table 3) are, generally, in good agreement with the data obtained from the well-polished phases of M45-ECC. The modulus of quartz, the most abundant well-polished phase and therefore the easiest to use as a standard, was measured to be 105.1 ± 9.3 GPa, similar to the values of 117 ± 3 and 104.2 ± 5.9 GPa measured by Whitney et al. and Zhu et al. [19,20], respectively.

The value of 120.4 ± 20.7 GPa measured for the modulus of unreacted fly ash is slightly higher than the 78.3 ± 14 GPa reported by Němeček et al. [18] This is likely due to differences in the composition of the fly ash, the manner in which the fly ash was processed, etc. The large standard deviation implies that the modulus of fly ash is, in general, rather variable. The measured modulus of PVA fibers (indented perpendicular to the fiber axis) is also very close to that reported by Němeček et al. Finally, the measured modulus of an alumina standard (76.2 ± 11.8) is close to the known modulus (73 GPa), and provides a good estimate of the error that can be expected in future tests (roughly 18%).

No distinction was made between the inner product (high density C–S–H) and outer product (low density C–S–H) in this study. It is known that the inner product, being closer to grains of clinker, contains more Ca, packs more efficiently, and has a higher modulus [3]. Nanoindentation experiments were performed at distances of <5, 10, 20, 30, and 50 μm from the edges of fibers so as to characterize the fiber/matrix interface. The expected distance from the edge of fibers

Table 3
Comparison of nanoindentation results from the literature and preliminary results.

Phase	E (GPa)[a]	Source
Quartz	117 ± 3	[19]
	104.2 ± 5.9	[20]
	105.1 ± 9.3	This author
Inner product [b]	31.4 ± 2.1	[20]
	29.4 ± 2.4	[3]
	30.4 ± 2.9	[7]
	34.2 ± 5.0	[26]
	22.97	[16]
	40[c]	[24]
Outer product	23.4 ± 3.4	[20]
	21.7 ± 2.2	[3]
	25.74 ± 10.84	[16]
	19.7 ± 2.5	[26]
	33.6 ± 11.6	[18]
	22.5 ± 5	[7]
	25[c]	[24]
"Ultra high density" C–S–H[d]	40.9 ± 7.7	[7]
PVA fiber [e]	10.6 ± 2.7	[18]
	7.3 ± 1.0	This author
Fly ash	78.3 ± 14	[18]
	120.4 ± 20.7	This author

[a] Some data does not include standard deviations.
[b] Also called 'high density' C–S–H; outer product also called 'low density' C–S–H.
[c] Inner product data point collected 5 μm from clinker particle; outer product collected 20 μm from clinker particle.
[d] A statistically-identified mixture of C–S–H and portlandite accounting for 19% of the hydrated phases is a sub-stoichiometric cement.
[e] Measured perpendicular to normal axis.

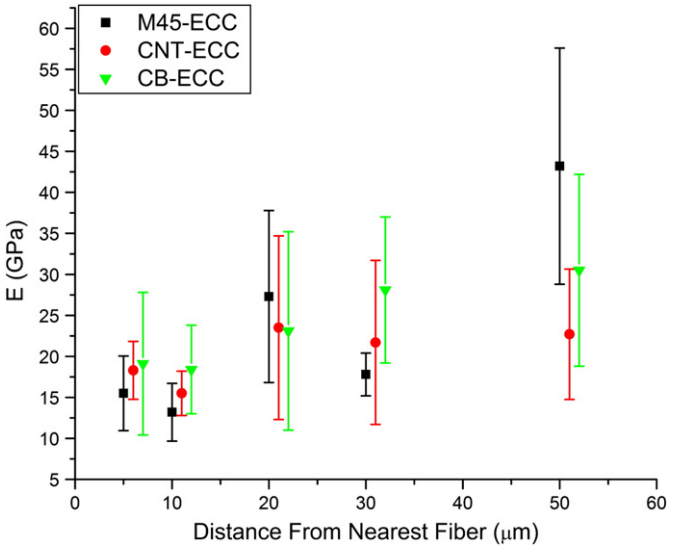

Fig. 2. E (GPa) as a function of distance from nearest fiber. All values were obtained at distances of <5, 10, 20, 30, and 50 μm from fibers; the slight offset is for display purposes only. Values at 50 μm are considered representative of 'bulk matrix' without any effect from the interfacial transition zones of fibers. At least 5 values were averaged for each data point.

and the actual distance, as measured by SEM, varied by less than roughly 1 μm. To ensure that fibers slightly beneath the surface would not affect the results, sample surfaces were polished perpendicular to fiber alignment. Therefore, the distance to the nearest fiber is certain. Effects from the transition zone between the cementitious matrix and sub-surface particles of unreacted fly ash cannot, however, be discounted. The obtained values are plotted in Fig. 2, while the exact values can be found in Table 4.

Close to the fibers (i.e. at <5 and 10 μm) the modulus of M45-ECC is at its lowest, 15.5 ± 4.6 and 13.1 ± 3.5 GPa, respectively. The modulus increases to 27.3 ± 10.5 GPa at 20 μm. Although the average modulus at 30 μm is lower (17.7 ± 2.6 GPa), the standard deviations of the modulus at 20 and 30 μm allow for some overlap. Finally, at a distance of 50 μm the modulus peaks at 43.2 ± 14.4 GPa. This value is roughly equivalent to that reported by Mondal et al. for high density C–S–H (41.5 ± 1.7 GPa) [24], while the lower values closer to the fibers (i.e. at 5, 10, 20 and 30 μm) are similar to values determined by various authors for inner- and outer-products (for a complete listing, see Table 3) (Fig. 3).

The measured modulus of 43.2 ± 14.4 GPa at a distance of 50 μm from the fiber in the M45 sample raises a further matter. A recent paper by Vandamme et al. [7] proposes the existence of a third important phase in the cementitious matrix; that of an Ultra High Density (UHD) phase, a mixture of C–S–H and portlandite, with a modulus of 40.9 ± 7.7 GPa. Identification of such a phase here, however, is complicated by two factors: the high standard deviations of both the 50 μm M45 data point measured here and of the UHD phase reported by Vandamme, and the lack of similar high moduli in the other two formulae, discussed below. The mean of the 50 μm M45 data point is, in fact, much higher than any other average value reported here; the origin of this high modulus (UHD C–S–H, experimental error, other phases, etc.) is a subject of ongoing investigation.

The standard deviations of these values, while quite large, are similar to those reported by Hughes and Trtik (25.74 ± 10.84 GPa) and Němeček et al. (33.6 ± 11.6) [16,18] for outer product C–S–H. Such large deviations effectively highlight the highly heterogeneous nature of the cement matrix, both in ECC and standard cementitious systems. Overall, the general trend is one of modulus that increases with distance from the fiber, rising sharply between 30 and 50 μm.

This general trend was also observed in the CB-ECC formula. The modulus was lowest at <5 and 10 μm from the fiber (19.1 ± 8.7 and 18.3 ± 5.4 GPa, respectively). The modulus increased in both value and standard deviation with distance from the fiber edge, until reaching a maximum of 30.4 ± 11.7 GPa at 50 μm. This value is lower than that measured for the M45-ECC, however, the relatively high standard deviations associated with both values provide a large amount of overlap.

In the CNT-ECC formula, this general trend was observed between <5 and 30 μm from the fiber. The values of modulus, as well as the standard deviations, are in the same range as those of the other two formulae. At 50 μm, however, the modulus does not increase, remaining at 22.6 ± 7.9 GPa. When standard deviation is taken into account, this value somewhat overlaps the CB-ECC data, but not the higher M45-ECC data. Why the modulus of CNT-ECC levels off in this manner, rather than increasing with distance from the fiber, is not clear. One possibility is that the areas selected for testing simply happened to be low density, and thus low–modulus, C–S–H; as multiple points were tested on multiple samples, this seems unlikely. While it is possible that some minor variation in the fabrication, mounting, or polishing of the sample led to lowered mechanical properties at this distance, a certain answer is not evident.

There are a number of explanations for why the modulus values generally increase with distance from the fiber:

1. Grains of unreacted cement are less likely to be found very near fibers due to the 'wall effect' [25]. The cementing phase near the fiber is therefore low density, Ca-deficient outer product, which is known to have a lower modulus [24]. In cements with high w/c ratios, this effect can also cause microbleeding, in which water collects under the fiber, decreasing the density and reducing the modulus. The wall effect could also explain why, near the fibers, the standard deviation of the data is lower in absolute terms: there is a much smaller chance of accidentally indenting a grain of quartz, unreacted fly ash, or unreacted cement close to a fiber. Microindentation techniques have shown that the hardness of the ITZ can be improved through the use of highly reactive silica fume, which will react with any free $Ca(OH)_2$ to produce high-Si C–S–H with reduced porosity.
2. The PVA fibers, being hydrophilic, are coated with a proprietary oiling agent to tailor the level of fiber/matrix bonding. Because the fiber is not solidly bonded to the matrix, during polishing the fiber might vibrate, causing deterioration of the surrounding area [18]. The qualitative observation that the fiber/matrix ITZ does not seem rougher when observed in the SEM is offered. Microindentation techniques have shown that the use of polymers [15], which will fill cracks and voids, efficiently combats such behavior.

A reduced-modulus ITZ, common in ECC and ordinary fiber-reinforced cement composites, is not observed in Ultra High Performance Concrete (UHPC) materials reinforced by steel fibers [26]. In such systems, the amount of high density C–S–H is maximized through the use of siliceous admixtures, producing a stronger fiber/

Table 4
Nanoindentation results of M45 ECC, CB-ECC, and CNT-ECC as a function of distance from nearest fiber. Indentations of the interfacial transition zone between cementitious matrix and particles of unreacted fly ash (FA-ITZ) were made at a distance of 10 μm from the nearest fly ash particle. The numbers in parenthesis are the number of successful indents from which data was collected.

Distance	M45-ECC	CNT-ECC	CB-ECC
5	15.5 ± 4.6 (5)	18.3 ± 3.5 (5)	19.1 ± 8.7 (5)
10	13.1 ± 3.5 (7)	15.4 ± 2.7 (10)	18.3 ± 5.4 (9)
20	27.3 ± 10.5 (5)	23.5 ± 11.2 (4)	23.1 ± 12.1 (9)
30	17.7 ± 2.6 (5)	21.7 ± 10 (7)	28.1 ± 8.9 (9)
50	43.2 ± 14.4 (9)	22.6 ± 7.9 (9)	30.4 ± 11.7 (9)
FA-ITZ	24.9 ± 6.6 (3)	39.1 ± 22.6 (3)	20.5 ± 5.4 (5)

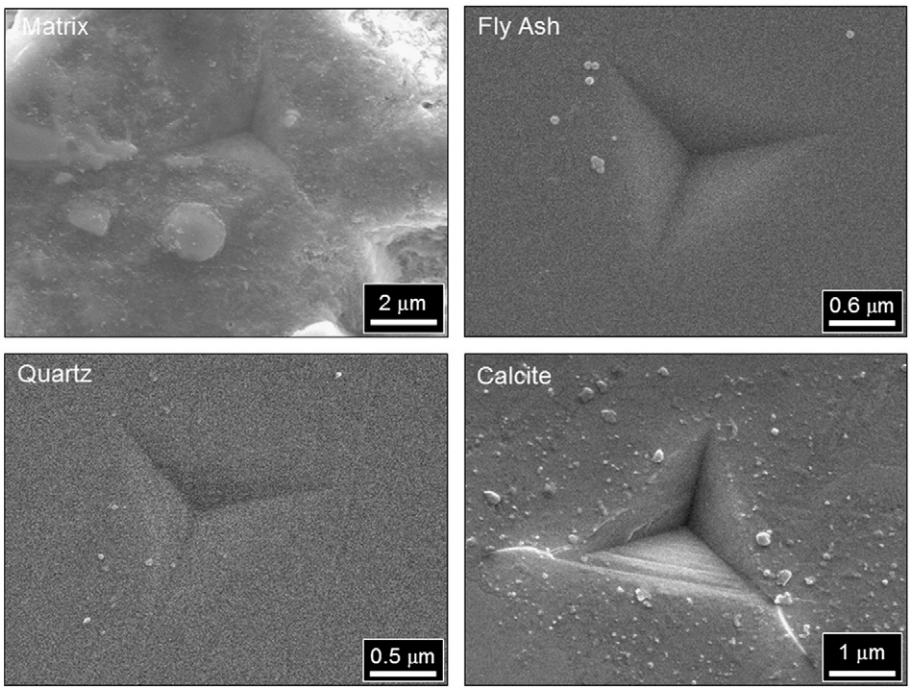

Fig. 3. SEM images of indents in several phases found in ECC.

matrix interface. Systems with similar steel fibers, but not optimized for high density C–S–H, behave like ECC (with a weakened ITZ) [25].

Indents were also made at a distance of 10 μm from the interface between the matrix and particles of unreacted fly ash (Table 4). Because unreacted fly ash is spherical, and can be positioned anywhere in the body of a 3-dimensional sample, the influence of phases just below the surface of the samples cannot be judged. As such, indents were carried out at this distance only.

The observed moduli, as with the matrix near fibers, are generally lower than the modulus of the bulk matrix: 24.9 ± 6.6 GPa for M45-ECC, 20.5 ± 5.4 GPa for CB-ECC, and 39.1 ± 22.6 GPa for the CNT-ECC. This last value, the average of three points, has a quite high deviation, and is therefore suspect. These three indents were never located in the SEM; it is possible that the matrix/fly ash ITZ was not indented, rather, the indents landed on (or partially on) fly ash particles, artificially raising the observed modulus. It is also possible that the indent was performed on a high-modulus phase, such as quartz, partially hidden under a thin layer of cementitious matrix. The moduli of the other two formulae are reasonably similar to each other and are within the range of moduli measured approaching fibers.

As with the fiber ITZ, there are two possible reasons for this decrease in modulus: first, fly ash particles provide a substantial dosage of Si due to their pozzolanic properties. This, in turn, produces low-modulus, Ca-deficient gel. Second, the extremely hard fly ash particles vibrate during polishing and may cause microcracking or residual stresses, which in turn may artificially lower the modulus.

Overall, the results of the indentation experiments serve to justify the polishing method selected for this work. The standard deviation of the polished alumina standard is 15%; the deviation at each distance from a fiber is roughly 30%. Much of this deviation is likely due to no distinction being made between low- and high density C–S–H, which are known to have different moduli. That the data is in the same range as what is reported in the literature for cement and what little data exists for ECC, is a second indirect check. The most powerful check was the plotting of each load/displacement curve to check for signs of irregularity due to roughness. However, work continues to develop more advanced polishing regimes, so as to separate deviation due to cement inhomogeneity from deviation due to roughness.

3.3. Electron microscopy

Polished, nanoindented samples were observed in the SEM. Despite their small size (only 500 nm deep), it was possible to find many of the indents (Fig. 2). Locating indents on well-polished phases was much easier than locating indents in the matrix. Indents in brittle materials, such as an errant grain of calcite, showed some cracking at the tips of the triangular indents. Such cracking was occasionally seen in the matrix, however, these cracks were not sufficient for calculating fracture toughness, which can be performed using crack length [19].

EDS was used to determine the elemental composition at 12 indent sites in the M45-ECC sample. The Ca/Si ratio of the cement matrix varied between 0.7 and 2.2 (average 1.5 ± 0.6) and had no readily apparent correlation to modulus. While the indents are only 500 nm deep, the X-rays that produce EDS signal are collected from a volume of up to several cubic microns. Therefore, phases under the surface that do not affect nanoindentation results could contribute to the EDS data.

12 points is not optimal for a truly statistic representation of the modulus of cement; however, these sites represent areas where indents left behind by the nanoindentation experiment could be positively identified. From the unloading portion of the load/displacement curve, it is clear that the cementitious material exhibits a elastic response, 'relaxing' after the load is withdrawn, either making the residual indentation so small as to be difficult to locate, or altering the triangular shape of the indent to the extent so that it is difficult to recognize. Though not conclusive, the EDS results, when combined with what is known of high- and low density C–S–H, imply that chemical composition has less of an effect on modulus than other parameters, such as porosity of C–S–H or the efficiency of packing the individual C–S–H grains.

Fracture surfaces of the formulae containing carbon black and carbon nanotubes were also investigated by SEM. Particles of carbon black could not be located, no clumps or agglomerations were observed, and the fiber/matrix interface looked similar to that observed in M45-ECC. While not conclusive, these observations imply that the carbon black is well dispersed and does not aggregate on the fiber surfaces or agglomerate into large particles.

Nanotubes were easily located, and quite abundant, in the ultrafine (100–500 nm wide) cracks located near PVA fibers that had been peeled away from the matrix (Fig. 4a and c). Numerous nanotubes could be easily located in any given crack in this area. In similar-size cracks elsewhere in the bulk matrix of CNT-ECC, nanotubes were only rarely found, if at all (Fig. 4b) Though not conclusive, this observation implies that the nanotubes consolidate around the PVA fibers, and may aid overall mechanical properties by bridging cracks and 'reinforcing' the microcracks that propagate radially from the PVA fibers. At low magnification (Fig. 4d), many nanotubes could be observed protruding from either crack face, including some bridging nanotubes. At high magnification (Fig. 4e and f) these nanotubes could be more clearly observed and their crack-bridging nature confirmed. It should be noted that the sample was sputter coated with a thin layer of gold before observation; this may have added up to roughly 10 nm to the thickness of the nanotubes.

4. Conclusions

A number of conclusions about the use of nanoindentation in ECC can be drawn from this study:

1. Pure cementitious matrix, far from the influence of PVA fibers, has the highest modulus (~30 GPa), which decreases nearer to fibers or particles of unreacted fly ash. The 'interfacial transition zone' around the PVA fibers is roughly 30 μm wide (that of the ITZ between cement matrix and unreacted fly ash was not measured). The lowered modulus in this zone is likely due to a combination of reduced Ca content, the associated alteration of pore structure, and complications due to polishing difficulties (i.e. surface roughness or microcracking).
2. Elemental analysis by EDS did not reveal any apparent correlation between Ca/Si ratio and modulus, therefore, it is more likely that

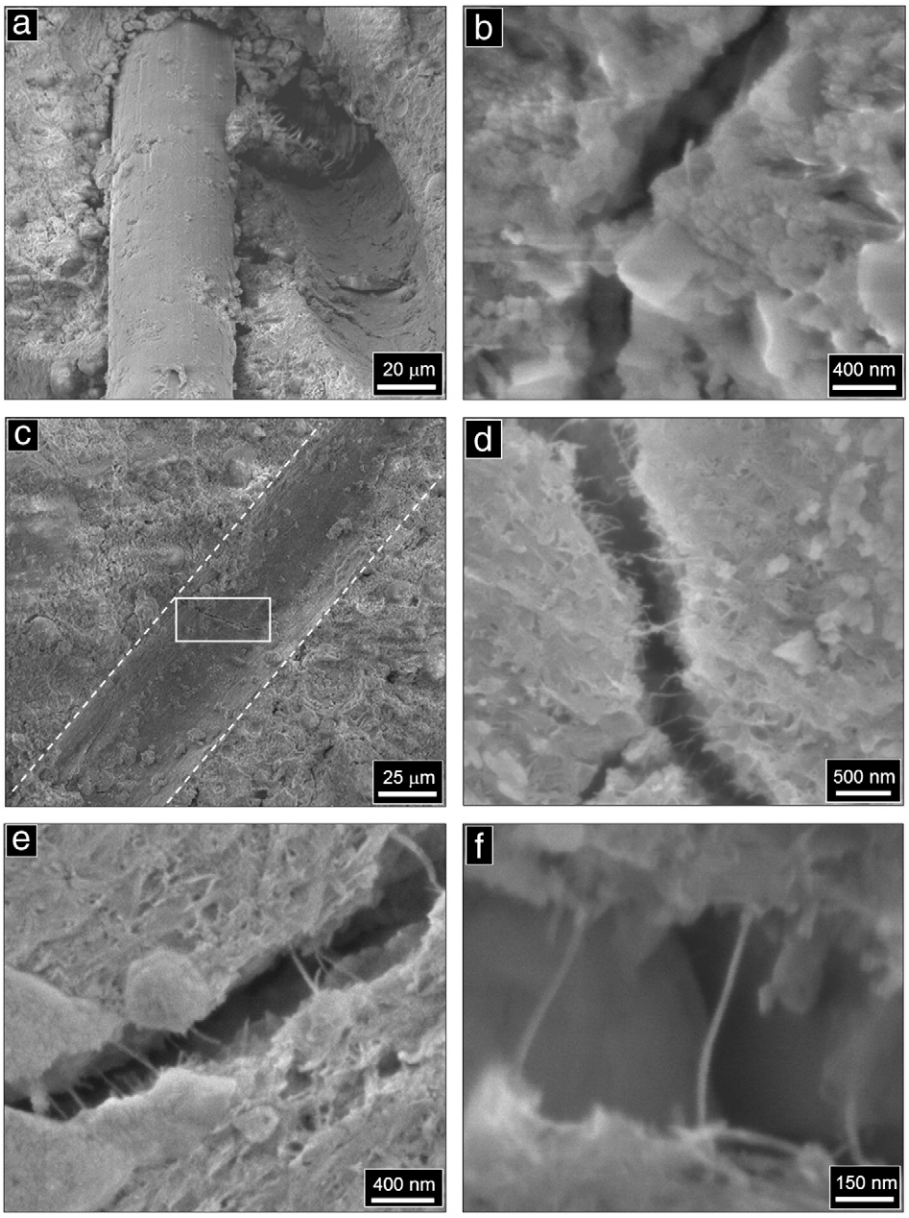

Fig. 4. SEM images of CNT-ECC. a) Fiber embedded in cement matrix (left) next to the pullout zone of another fiber (right); b) an ultrafine crack in the bulk matrix of CNT-ECC, far from fibers, in which nanotubes are not observed; c) Low-magnification view of the fiber pullout zone in which nanotubes were found to be plentiful. Dashed lines indicate original orientation of fiber. Images of nanotubes were taken from an ultrafine crack outlined in the white box; d) overview of ultrafine crack, showing abundance of nanotubes; e) higher magnification image of an ultrafine crack with several bridging nanotubes; f) an individual bridging nanotube.

nanoscale mechanical properties are more strongly affected by properties such as porosity and degree of hydration.

3. The inability to locate carbon black suggests even dispersion of these particles, while the ease of finding carbon nanotubes in cracks near fiber pullout zones implies a certain degree of agglomeration of nanotubes around the PVA fibers.
4. While the moduli data pertaining to the ECC formulae containing carbon black and carbon nanotubes varies somewhat, overall, the inclusion of these additives did not negatively affect the nanoscale mechanical properties of the ECC. Therefore, it is likely that these materials can easily and successfully be used to tune the electrical properties of ECC, without negative consequence on the nanoscale, for future applications.

Despite the difficulties in obtaining well-polished samples and reliable data, nanoindentation is a useful technique that can be used to determine the effects of various nanomaterial additives on local mechanical properties. In turn, this information may someday be used in micromechanical models that treat ECC as a highly heterogeneous nanocomposite and spur the development of future ECC formulations.

Acknowledgements

The authors would like to gratefully acknowledge the generous support of the U.S. Department of Commerce, National Institute of Standards and Technology (NIST) Technology Innovation Program (TIP) under Cooperative Agreement Number 70NANB9H9008. Additional support was provided by the University of Michigan, and by the US National Science Foundation under grant CMMI-0700219.

References

[1] V.C. Li, On engineered cementitious composites (ECC): a review of the material and its applications, Journal of Advanced Concrete Technology 1 (2003) 215–230.
[2] H. Lindgreen, M. Geiker, H. Krøyer, N. Springer, J. Skibsted, Microstructure engineering of Portland cement pastes and mortars through addition of ultrafine layer silicates, Cement & Concrete Composites 30 (2008) 686–699.
[3] G. Constantinides, F.-J. Ulm, The effect of two types of C–S–H on the elasticity of cement-based materials: results from nanoindentation and micromechanical modeling, Cement and Concrete Research 34 (2004) 67–80.
[4] P. Mondal, S.P. Shah, L. Marks, Nanoscale characterization of cementitious materials, ACI Materials Journal 105 (2008) 174–179.
[5] G. Constantinides, F.-J. Ulm, K. Van Vliet, On the use of nanoindentation for cementitious materials, Materials and Structures 36 (2003) 191–196.
[6] M. Vandamme, F.-J. Ulm, Nanogranular origin of concrete creep, Proceedings of the National Academy of Sciences 106 (2009) 10552–10557.
[7] M. Vandamme, F.-J. Ulm, P. Fonollosa, Nanogranular packing of C–S–H at substochiometric conditions, Cement and Concrete Research 40 (2010) 14–26.
[8] S. Wang, V.C. Li, Engineered cementitious composites with high-volume fly ash, ACI Materials Journal 104 (2007) 233–241.
[9] S. Qian, J. Zhou, M.R. de Rooij, E. Schlangen, G. Ye, K. van Breugel, Self-healing behavior of strain hardening cementitious composites incorporating local waste materials, Cement & Concrete Composites 31 (2009) 613–621.
[10] LepechM. , Improving infrastructure sustainability using nanoparticle engineered cementitious composites. In International conference on advanced concrete materials, CRC Press, Stellenbosch, South Africa, 2009.
[11] G.Y. Li, P.M. Wang, X. Zhao, Mechanical behavior and microstructure of cement composites incorporating surface-treated multi-walled carbon nanotubes, Carbon 43 (2005) 1239–1245.
[12] S. Wen, D.D.L. Chung, Partial replacement of carbon fiber by carbon black in multifunctional cement-matrix composites, Carbon 45 (2007) 505–513.
[13] J. Chen, C.S. Poon, Photocatalytic construction and building materials: from fundamentals to applications, Building and Environment 44 (2009) 1899–1906.
[14] S. Wei, Effect of addition of silica fume and polymer on the interfacial layer between steel fiber and cement matrix, Journal of The Chinese Ceramic Society 15 (1987) 503–509.
[15] S. Wei, J.A. Mandel, S. Said, Study of the interfacial strength in steel fiber-reinforced cement-based composites, ACI Journal 83 (1986) 597–605.
[16] J.J. Hughes, P. Trtik, Micro-mechanical properties of cement paste measured by depth-sensing nanoindentation: a preliminary correlation of physical properties with phase type, Materials Characterization 53 (2004) 223–231.
[17] J. Nemecek, Creep effects in nanoindentation of hydrated phases of cement pastes, Materials Characterization 60 (2009) 1028–1034.
[18] J. Němeček, Petr Kabele, Z. Bittnar, Nanoindentation based assessment of micromechanical properties of fiber reinforced cementitious composite, 6th RILEM Symposium on Fibre-Reinforced Concretes (FRC)—BEFIB 2004, RILEM, Varenna, Italy, 2004.
[19] D.L. Whitney, M. Broz, R.F. Cook, Hardness, toughness, and modulus of some common metamorphic minerals, American Mineralogist 92 (2007) 281–288.
[20] W. Zhu, J.J. Hughes, N. Bicanic, and C.J. Pearce, Nanoindentation mapping of mechanical properties of cement paste and natural rocks, Materials Characterization. 58 (2007) 1189-1198.
[21] W.C. Oliver, G.M. Pharr, An improved technique for determining hardness and elastic modulus using load and displacement sensing indentation experiments, Journal of Materials Research 7 (1992) 1564–1583.
[22] ASTM, E2546. 2007, American Society for Testing Materials: Philadelphia, PA.
[23] P. Trtik, J. Dual, B. Muench, L. Holzer, Limitation in obtainable surface roughness of hardened cement paste: 'virtual' topographic experiment based on focussed ion beam nanotomography datasets, Journal of Microscopy 232 (2008) 200–206.
[24] P. Mondal, S.P. Shah, L. Marks, A reliable technique to determine the local mechanical properties at the nanoscale for cementitious materials, Cement and Concrete Research 37 (2007) 1440–1444.
[25] X.H. Wang, S. Jacobsen, J.Y. He, Z.L. Zhang, S.F. Lee, H.L. Lein, Application of nanoindentation testing to study of the interfacial transition zone in steel fiber reinforced mortar, Cement and Concrete Research 39 (2009) 701–715.
[26] L. Sorelli, G. Constantinides, F.-J. Ulm, F. Toutlemonde, The nano-mechanical signature of ultra high performance concrete by statistical nanoindentation techniques, Cement and Concrete Research 38 (2008) 1447–1456.